

МИНЕРАЛОГИЯ ЛУННЫХ НЕДР И МОДЕЛИРОВАНИЕ ПРОФИЛЯ ПЛОТНОСТЕЙ НА ОСНОВЕ ДАННЫХ СПЕКТРОМЕТРА M³

В. Чжан^{1,2}

¹ Department of AOP Physics, University of Oxford, Wellington Square, Oxford OX1 2JD, United Kingdom

² Department of Mathematics, Physics and Information, Shaoxing University,
No.508, Huancheng West Road, Shaoxing, 312000, China

После рассмотрения методов определения содержания FeO и Ti₂O по данным космического зонда «Клементина» (Clementine) разработан авторский подход к установлению этих составов с помощью измерений, сделанных инструментом M³ на зонде «Чандраян-1» (Chandrayaan-1). На основании информации о содержании FeO и Ti₂O смоделирована плотность пород, подстилающих лунный грунт. Данные о концентрации FeO и Ti₂O, полученные инструментом M³, сопоставлены с данными зонда «Клементина» и установлена их хорошая сходимость. Концентрации FeO также хорошо согласуются с результатами исследований станции «Лунный геолог» (Lunar Prospector), которые использовались как независимый источник. Предыдущие данные зонда «Клементина» и новые данные, полученные инструментом M³, сравнивались с лабораторными измерениями содержаний FeO и Ti₂O в образцах, взятых при проведении программ «Аполлон» и «Луна». Содержание FeO, по данным зонда «Клементина», стабильно ниже данных лабораторных измерений на 1—2 %. Концентрации, полученные инструментом M³, лучше соответствовали лабораторным измерениям образцов из программы «Аполлон» (±2.8 %). Содержание Ti₂O, по данным зонда «Клементина», стабильно ниже данных лабораторных измерений на 0.1—4 %. Концентрации Ti₂O, по данным инструмента M³, близки к данным лабораторных измерений (±0.6 %), кроме отдельных образцов с высоким содержанием Ti₂O. Однако следует с осторожностью интерпретировать эти результаты, так как требуется более тщательное исследование диапазона погрешности. К сожалению, к данным зонда «Клементина» не был предоставлен анализ ошибок определения.

Моделирование профиля плотностей, приповерхностный слой Луны, данные космических зондов, данные M³

LUNAR SUBSURFACE MINERALOGY AND DENSITY PROFILE MODELING BASED ON M³ DATA

W. Zhang

Methods of deriving FeO and TiO₂ contents from Clementine spacecraft data are discussed, and our own approach is developed for deriving the contents from measurements made by the M³ instrument on Chandrayaan-1. The density of lunar soil bedrock is modeled based on the derived FeO and TiO₂ information. The FeO and TiO₂ abundance we derived from the M³ data is compared with previous results from the Clementine data and is in good agreement. The FeO abundance data also agree well with the Lunar Prospector data, which were used as an independent source. The previous Clementine and new M³-derived abundances are compared with the laboratory-measured FeO and TiO₂ contents in the Apollo and Luna returned samples. The Clementine-derived FeO content was systematically 1—2% lower in all the returned samples than the laboratory measurements. The M³-derived content agrees better with the returned Apollo samples and is within ±2.8% of the laboratory-measured ones. The Clementine-derived TiO₂ abundance is systematically 0.1—4% higher than the laboratory measurements of the returned samples. The M³-derived TiO₂ content agrees well (±0.6%) with the laboratory measurements of the returned samples, except for the samples with a high TiO₂ content. However, caution should be taken when interpreting these results, as the error range needs further study. Unfortunately, no error analysis was provided with the previous Clementine-derived contents.

Density profile modeling, lunar subsurface, Spacecraft data, M³ data

COMMONLY USED ABBREVIATIONS

Below is a list of abbreviations seen in the text; some with a small description. All are defined throughout the paper, but are also listed here for quick reference: LRO, Lunar Reconnaissance Orbiter; MRM, Microwave Radiometer; M³, Moon Mineralogy Mapper.

© В. Чжан✉, 2019

✉e-mail: zhangw@physics.ox.ac.uk

DOI: 10.15372/GiG2019127

INTRODUCTION

Missions exploring the lunar surface have greatly improved our understanding of the Moon's composition, origin and evolution. Over geologic time, the lunar surface has been shaped by impacts, solar irradiation and cosmic rays. After the Apollo and Luna landings in the 1970s, subsequent lunar exploration mainly used visible and infrared remote sensing to study the topography, composition and near-surface thermal properties of the Moon.

However, information about the properties of the lunar subsurface and deep structural features are hard to determine, except for measurements obtained at the Apollo and Luna landing sites and from returned lunar samples (Lunar Source Book, 1991). Geochemical surveys of returned lunar samples cannot provide direct information on the global composition and physical properties of the subsurface. As a result, knowledge of the Moon's basic geophysical properties, including its internal structure, which can help in constraining theories about its formation and evolution, remains lacking, and our understanding of the lunar origin and evolution is still limited (Hartmann, 1986). Due to these limitations, the lunar subsurface mineralogy, deep structural features and thermal environment are still not fully understood.

The first part of this paper is therefore concerned with the development of a method for deriving FeO and TiO₂ content from the data measured by the Moon Mineralogy Mapper (M³) instrument (Fig. 1a) on the Chandrayaan-1 mission.

The FeO and TiO₂ spatial distribution across the lunar surface was originally mapped by the Clementine ultraviolet-visible/near-infrared (UV/VIS/NIR) spectrometer (Nozette et al., 1994) and in this chapter it will be further mapped by the M³ instrument.

Data from M³ contains a wider spectral range from approximately 430 to 3000 nm (more compositional information), higher spatial (up to 70 m/pixel target mode, 140 to 280 m/pixel global mode, while the Clementine is 1 km/pixel) and spectral resolution (256 channels target mode, 85 channels global mode, while Clementine only has 5 channels) (Pieters et al., 2009) and has a more well defined calibration scheme than Clementine data (Clark et al., 2010). The mission started in October 2008 and ended in late August 2009. 95% of the Moon is covered in its global mode (Boardman et al., 2011) as shown in Fig. 1b below. Therefore, it has significant potential advantages when compared with previous products derived from the Clementine mission and ground-based observations. These advantages of the M³ data provide an opportunity to improve the accuracy of previous global elemental abundance maps derived from Clementine (which had large uncertainties) and also provide an important test of different reduction approaches (Lucey et al., 1995, 1996, 1998, 2000; Blewett et al., 1997; Pinet et al., 1997; Shkuratov et al., 1999). This research tests the validity of the Clementine-derived maps and Ti/Fe composition models.

Despite the potential for improvement over the Clementine dataset, there are factors complicating the data reduction process that need to be discussed. First, the M³ dataset is large (3.63 TB), requiring a long time for the completion of data reduction, in particular reformatting the data requires about 1 month on a typical desktop computer. Secondly, the M³ dataset contains several known anomalies. The Chandrayaan-1 spacecraft experienced a diverse range of non-nominal thermal and field-of-view (largely pointing) conditions while acquiring the M³ data (Boardman et al., 2011). Solar illumination of the lunar surface affected the measured signal level, strongly affecting the spacecraft environment and operations, and consequently affected the temperature of the M³ detector. Several data correction programs were developed to address such limitations by removing noise sources, repairing banded anomalous data tracks and cleaning up the data (Kim et al., 2016).

Additional details of the operation aspects of the M³ instrument during lunar mapping are given by Boardman et al. (2011), and details of the M³ instrument design and capabilities are presented by Green et al. (2011). Calibrated M³ data can be downloaded from the NASA PDS node: <http://pds-imaging.jpl.nasa.gov/volumes/m3.html>.

LUNAR SURFACE MINERALOGY RETRIVAL

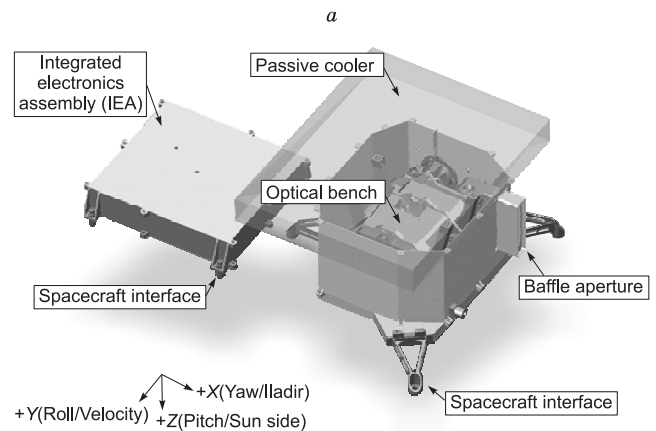
Overview of previous Ti and Fe retrieval methods

The abundance and spatial distribution of both Ti and Fe is important in understanding the petrogenesis of lunar rocks and thus, the nature and origin of the Moon (Lucey et al., 1998).

The VIS-NIR reflectance characteristics of the Moon are sensitive to chemical, mineralogical and physical properties of lunar regolith and have been widely used in lunar geological explorations (Lucey et al., 2006). Many models have been suggested to quantify Fe and/or Ti abundances from Clementine's UV/VIS images (Lucey et al., 1995, 1998, 2000; Blewett et al., 1997; Lawrence et al., 2002a,b; Gillis et al., 2004). None of the authors provided content retrieval errors of Clementine FeO or TiO₂ abundances in their papers (Lucey et al., 1995, 1996, 1998, 2000; Blewett et al., 1997; Shkuratov et al., 1999). Among these models, Lucey's model (Lucey et al., 1995, 1996, 1998, 2000) has been one of the most popular and has undergone a series of refine-

Fig. 1. (a), M³ that flew on board on India's Chandrayaan-1 mission from October 2008 through August 2009 (Boardman et al., 2011).

Compared with Clementine, M³ contains a wider spectral range (Boardman et al., 2011; Green et al., 2011). The size of M³ instrument main body is 40 cm × 30 cm. (b), Coverage of M³ dataset in global mode, containing all available optical periods. Blue indicates the signature of water, green shows the brightness of the surface, and red indicates iron-bearing minerals.



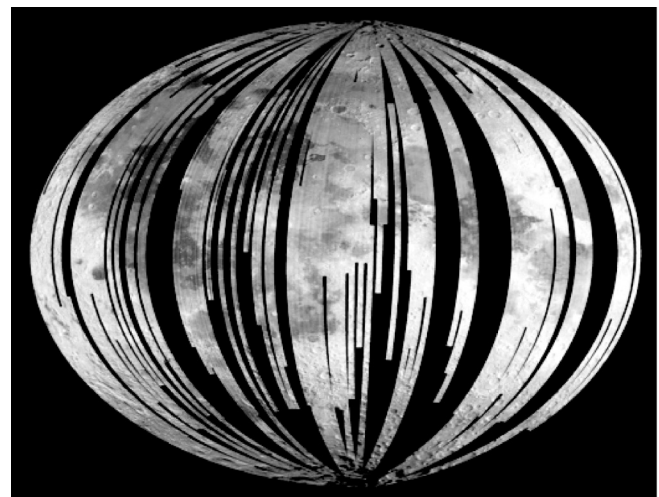
ments. As more mission datasets become available (e.g., Kaguya from Japan, Chang'E-1 from China, Chandrayaan-1 from India, and Lunar Reconnaissance Orbiter from United States) (Pieters et al., 2008), a comparison of the results from these datasets as well as the refinement of FeO mapping algorithms will continue to improve global map estimates of Fe/Ti abundances. Previous efforts by other authors to derive compositional information on lunar FeO and TiO₂ abundance from spectrometry were briefly reviewed by Lucey et al. (1995, 1998) and are summarized here.

Lucey et al. (1995) introduced a method to determine the Fe content of the lunar surface using the Clementine reflectance data at 750 nm and the ratio of reflectance at 950 nm (NIR) and 750 nm (VIS). Lucey et al. (1995) noted a trend with Fe content and maturity in the NIR/VIS ratio versus the VIS reflectance for returned lunar samples (Fig. 2). Lucey et al. (1995) placed an origin near the intersection of these maturity trends, and a characteristic spectral angular parameter was used to estimate composition information. Such an angular parameter was defined for the location of a sample in the ratio-reflectance plot as the angle between a horizontal line through the origin and a line defined by the origin and the location of each point on the plot (Fig. 2). The relationship between the Fe content and the angular parameter of the samples was used to provide the composition. Lucey et al. (1995) produced a global image of lunar Fe abundance by applying these relationships to early Clementine UV/VIS multispectral data.

Current research on determining the Ti abundance of the lunar surface using M³ data is limited (Dhingra et al., 2010). As M³ does not have the 415 nm channel which was used by Lucey et al. (1998) to retrieve Ti, I examined two different approaches to derive the abundance and distribution of lunar Ti in this chapter: (1) using the methods of Shkuratov et al. (1999) and (2) revising Lucey et al. (1998) by adapting the method to the M³ spectral channels. The first approach was validated within Shkuratov et al. (1999). The second approach was validated using ground truth from both Apollo data and samples from various Apollo landing sites. After adding this a priori elemental information to the radiative transfer model, the results were used to calculate spatial variations in the density of the lunar soil bedrock in part 3.

Iron content retrieval

To recap, using the data from the Clementine instrument, Lucey et al. (1995) applied the spectral characteristic angle method which is based on the following phenomena: (1) an absorption band of 750 nm—the 750 nm reflectance decreases with the increase of lunar soil maturity; (2) the ratio of reflected 950 nm/750 nm, which increases with lunar soil maturity; (3) both the overall reflectance of 750 nm and the ratio of R950/R750 (Fig. 2) decrease as Fe increase; and (4) the position of the origin depicted (at 1% reflectance and a ratio of 1.26 in Fig. 2) was optimized to maximize the linear correlation between the characteristic angle parameter and bulk iron content, hence is named as the “optimized origin” or “apparent origin”. Lucey et al. summarized these effects on the spectral slope by developing plots that are similar to those shown in Fig. 2, which were cited from (Lucey et al., 1995). Based on the above characteristics, Lucey et al. (Lucey et al., 1995; Blewett et al., 1997)



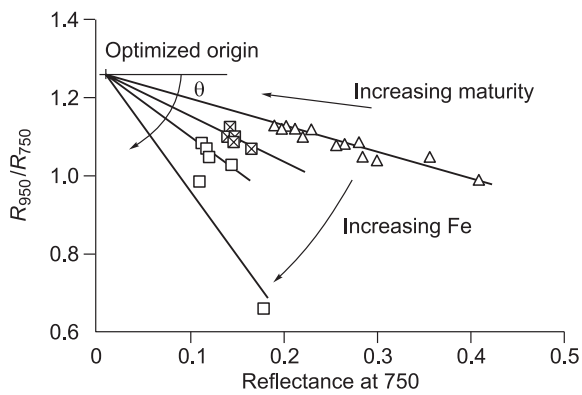


Fig. 2. Triangles are Apollo 16 soils; boxes are Apollo 15 soils. The contrasting spectral behavior of maturity and total Fe is clearly illustrated.

The Lucey method is based on following facts: (1) an absorption band of 750 nm—the 750 nm reflectance decreases with the increase of lunar soil maturity; (2) the ratio of reflected 950 nm/750 nm increases with lunar soil maturity; (3) both the overall reflectance of 750 nm and the ratio of R_{950}/R_{750} decrease as Fe increase; and (4) the position of the origin depicted was optimized to maximize the linear correlation between the characteristic angle parameter and bulk iron content, hence is named as the “optimized origin”.

developed the spectral characteristic angle method for FeO content retrieval while mapping Clementine UV/VIS data.

The formula to calculate FeO content is provided as follows (Lucey et al., 1995):

$$\theta_{\text{Fe}} = -\arctan\left(\frac{R_{950}/R_{750} - 1.26}{R_{750} - 0.01}\right). \quad (1)$$

$$\text{FeO}\% = 17.83 \times \theta_{\text{Fe}} - 6.82. \quad (2)$$

All data in Eqs. 1 and 2 are available and can be extracted from M^3 data. However, M^3 data were resampled to fit the Clementine instrument’s spectral grid for better precision using Matlab’s interpolation function. The difference is smaller than 1% (Fig. 3). Hence, applying Lucey’s et al. model, which was originally derived for Clementine data, for use with the M^3 dataset is reasonable.

I analyzed the FeO content based on M^3 data according to Eqs. 1–2. Lunar FeO content varies from 0 wt.% to 20 wt.% (Fig. 4a). However, the upper limit of 20% is a limitation of the model from Lucey et al. (1995, 1998) related to band-depth saturation of laboratory spectra of terrestrial mineral samples. The new result has been compared to the Clementine Fe retrieval map to validate these methods and show the datasets are consistent (Fig. 4a). From Fig. 4a it is possible to see visually that the two sets are in general agreement. There are some artifacts in the derived FeO distribution from the M^3 dataset due to the different optical periods used and the lack of complete global coverage. However, further comparative analysis is not possible as Lucey et al. (1995, 1998) did not provide any error estimations for their retrievals.

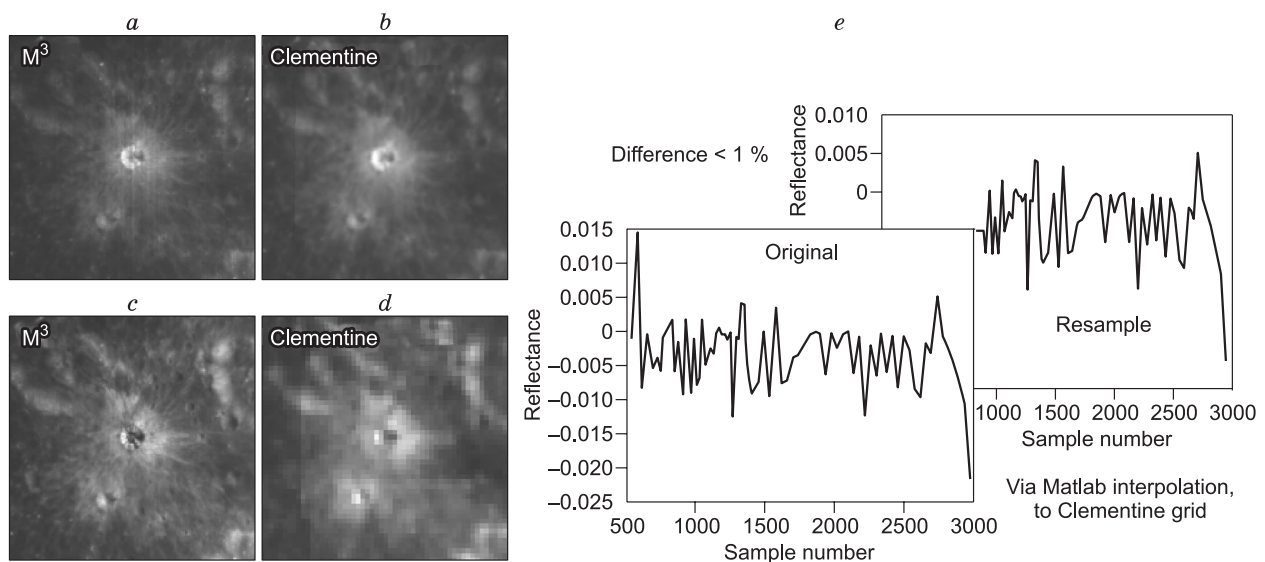


Fig. 3. Zoom of small crater located at $\sim 3.5^\circ$ S and 35.5° E.

Each frame is 6.8 km across. Selected to compare spatial resolutions of (a) M^3 at 750 nm reflectance and (b) Clementine’s UV-VIS camera at 750 nm reflectance, (c) M^3 at 2020 nm and (d) Clementine’s NIR camera at 2000 nm (a–d, are cited from (Kramer et al., 2011)); (e) resampling of M^3 data to Clementine grid. Comparison with original data shows that the difference is within 1%. Hence, Eqs. 1–2 can be used with M^3 . A random selection of 10 different spectra is used for demonstration.

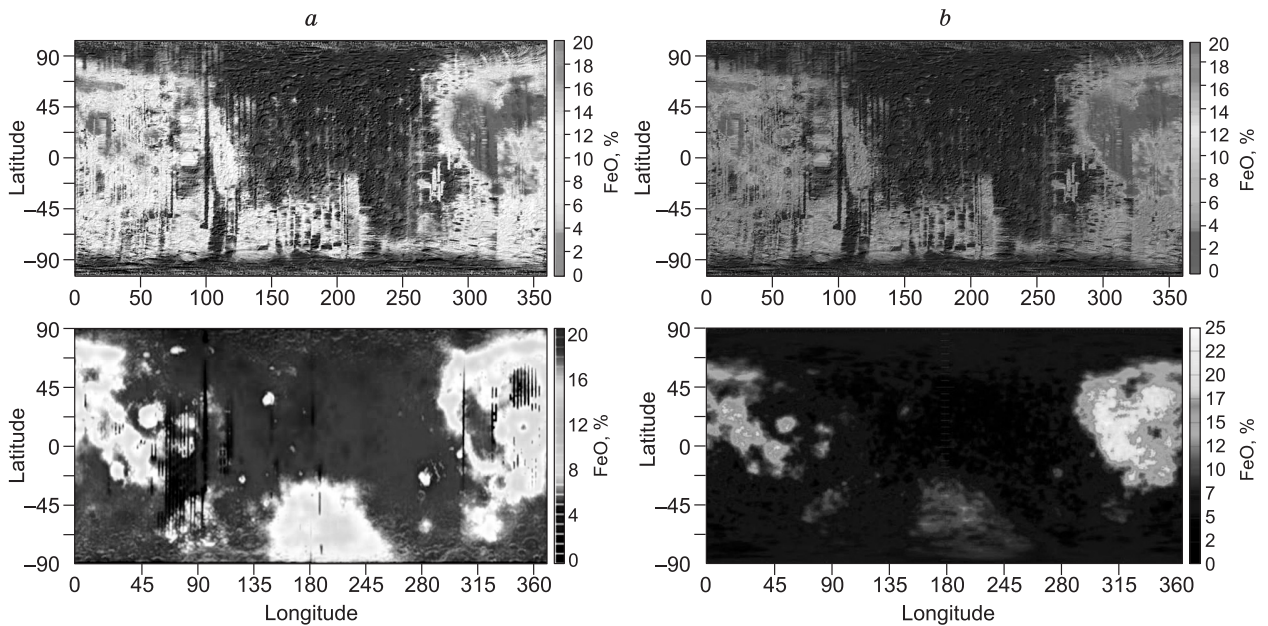


Fig. 4. (a), (Top) Retrieved FeO content from M³ over plotted on a Clementine base map.

Fe content is between 0–20% in this map. Several artifacts remain in this plot; they come from the M³ optical period; (bottom) Clementine FeO map. (b), Comparison of retrieval result of FeO content from the M³ (top, over plotted on a Clementine base map) with Lunar Prospector Fe map (below) (Lawrence et al., 2002a). Labels of scale bar: Fe%.

The derived Fe distribution from the M³ data has also been compared with the Lunar Prospector Fe mapping results in Fig. 4b. The Lunar Prospector dataset, which contains the first global measurements of gamma-ray spectra from the lunar surface, is the first direct measurement of the chemical composition of the entire lunar surface (Lawrence et al., 2002a,b, 2007). Hence, it differs from other remote sensing methods and is a good standard against which to check both the Clementine and M³ retrievals.

The Lucey et al. (1995, 1998) model has been compared with the Lunar Prospector FeO abundance map and they have been found to agree within $\pm 6\%$ (Lawrence et al., 2002a). Using this as a crude error analysis, the retrievals of the M³ and Clementine/Lunar Prospector are also consistent (within $\pm 6\%$). Such consistency validates the methods used. Several small features that are noticeable on the M³ are not seen on the Clementine or Lunar Prospector results, as the M³ has a much higher spatial resolution than the other two datasets. Furthermore, the M³ and Clementine results seem to have more artifacts than the Lunar Prospector, as the Lunar Prospector results are a more direct measurement (Lawrence et al., 2002a), appearing smoother due to a lower resolution.

Titanium content retrieval and methods

For the TiO₂ content retrieval, Lucey's et al. method (1998) also introduces a simple relation between the UV/VIS ratio (415 nm/750 nm) and TiO₂ content. However, an alternative method is required because the M³ does not include a 415 nm band. The 256 channels that are available in the M³ data allowed for investigation of other approaches that were inaccessible from the Clementine data, which were more spectrally limited. Two different TiO₂ analysis techniques were applied to the data and are described below.

First approach: Shkuratov model. Using a correlation diagram of FeO–TiO₂ for the lunar nearside, Shkuratov et al. (1999) studied the relationship between FeO and TiO₂ abundance. FeO% and $\log(\text{TiO}_2\%)$ have a high correlation coefficient of 0.81. The regression equation is as follows:

$$\log(\text{TiO}_2\%) = 0.06(\text{FeO}\%) - 0.54. \quad (3)$$

A comparison with the Clementine result is also provided in Fig. 5.

The Shkuratov method is a mathematical regression and has been validated by FeO and TiO₂ measurements from telescopic spectra and laboratory chemical data for the Apollo landing sites (Shkuratov et al., 1999).

The Shkuratov relationship (Shkuratov et al., 1999) can be explained for the lunar surface as ilmenite is the main TiO₂ bearing mineral and also contains FeO. Bhatt et al. (2011) also correlated FeO abundance to TiO₂

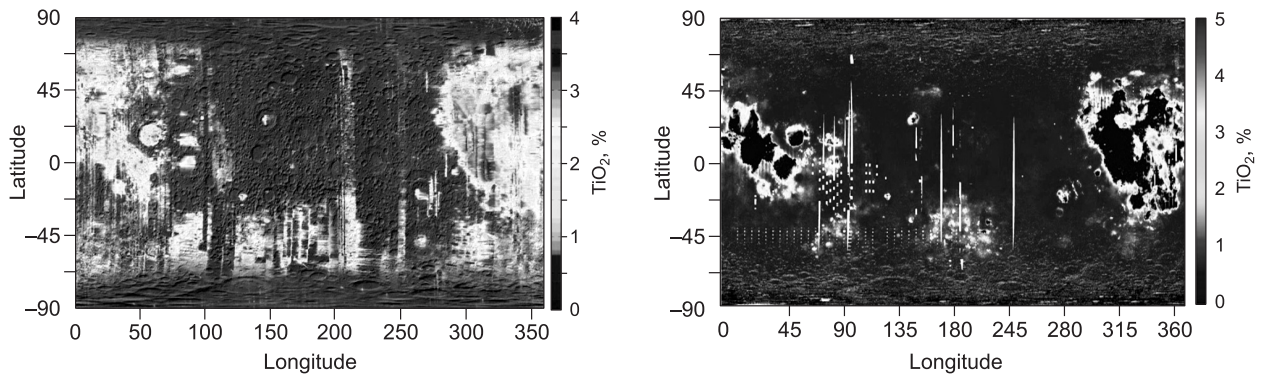


Fig. 5. (Left) Retrieval result of TiO₂ content derived using the Shkuratov model from the M³ FeO map shown in Fig. 4a, over plotted on a Clementine base map; (right) Clementine titanium map (Korokhin et al., 2008).

content (both in%) and absorption band parameters using data from an infrared spectrometer (SIR-2) on Chandrayaan-1:

$$\text{FeO}\% = 63.94 \times (\text{B} + 0.518 \times \text{S}) - 5.24 + 0.92 \text{TiO}_2 \%. \quad (4)$$

where B is absorption band depth and S is the continuum slope. The correlation factors are 0.90 and 0.96 for 2 μm and 1 μm absorption bands respectively. Such correlations may be related to early lunar geology, which has yet to be studied thoroughly.

Second approach: characteristic angle approach. A new preliminary model was developed in this research based on ground truths using the samples from Apollo and Luna sites. This model allowed for the production of a Ti abundance map from M³ images, which analyzes data by using a characteristic angle approach similar to that of Lucey et al. (1995). The principles of Lucey et al. (1995, 1998) were utilized, but were applied to M³ spectral bands, so the 540 nm channel was used instead of the 415 nm channel, which the M³ does not have.

Lunar Ti occurs mainly in the opaque mineral ilmenite (FeTiO₃) (Heiken et al., 1991). Ilmenite has distinctive reflectance characteristic in the UV/VIS spectrum. As seen in Fig. 6, ilmenite has two main absorption bands at 500 nm and 1500 nm. The 540 nm M³ spectral channel is close to the absorption center of the first band and the 750 nm M³ spectral channel is found near a reflectance maximum between two bands. The 500 nm band is principally due to the Ti³⁺ ion that is octahedrally coordinated to oxygen and is predicted to produce crystal-field bands in the visible region (Cloutis et al., 2008). This 540 nm position is also observed in lunar ilmenite sample 74220 (Vaughan and Burns, 1973) and was attributed to Ti³⁺ (Vaughan and Burns, 1973). Thus, using the nearby spectral channel (540 nm) of the M³ to predict the Ti content of the lunar surface is reasonable. The new model uses the M³ 540 nm (red line in Fig. 6) channel as a replacement for the 415 nm channel used in the Clementine retrieval. Both Clementine and M³ have a 750 nm channel (blue line in Fig. 6), so the wavelength used in the two techniques is the same.

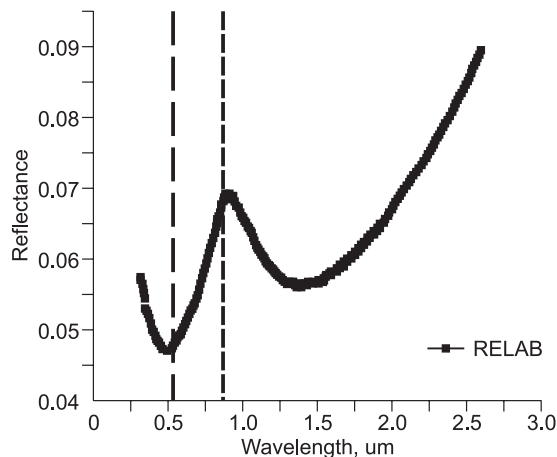


Fig. 6. UV/VIS/NIR spectrum of ilmenite from Brown University's RELAB (sample number: PI-CMP-006/C1PI06).

Available at: www.planetary.brown.edu/relabdata/data/cmp/pi/c1pi06.txt. This sample is representative of other samples in the RELAB ilmenite catalogue, and the observation geometry for the sample is the same as that of the M³ PDS data. The spectral range of M³ is 415 nm to 2,976 nm (0.4 μm to 3.0 μm). The red dashed line corresponds to the M³ 540 nm channel, and the blue dashed line corresponds to the M³ 750 nm channel.

Table 1. Selection criteria and reasoning of the M³ data used in the TiO₂ abundance analysis

Step	Criteria	Reason
1	Search for regions near Apollo and Luna lunar landing sites with the widest spread of TiO ₂ content. Apollo and Lunar landing sites with no TiO ₂ content are ignored	The largest range of TiO ₂ % is used to reduce error
2	Within the selected regions of Step 1, search for craters with a relatively small diameter (<10 km) and high albedo (>50%)	Small craters with high albedos are generally fresher and as a result are less likely to be contaminated by ejector blankets from other impacts
3	Within results of Step 2, find the craters that have distinct rays	Distinct rays in the crater ejecta also indicate relatively new craters. From the center outward along the radiation pattern, TiO ₂ content remains equal, whereas maturity increases
4	Within results of Step 3, find M ³ data points measured at 750 nm and 540 nm	Plotting the M ³ data using the same technique as Lucey et al. (1998) allows the characteristic spectral angular parameter to be calculated

Using the 540 nm and 740 nm M³ channels, a similar characteristic angle to Lucey et al. (1998) was calculated. The chemical contents of the lunar soil samples returned by the Apollo and Luna missions were then used as ground truths. This approach attempts to correlate the laboratory TiO₂ contents of typical lunar returned soils with the remotely sensed multispectral images using a technique based on Lucey et al. (1995, 1998, 2000). The criteria used to select the M³ data is outlined in Table 1.

All the available returned samples from the Apollo and Lunar missions whose landing sites were selected in step one (Table 1) were used in the data analysis. This was a total of 91 samples including 68 from the Apollo missions and 23 from the Luna missions. Due to the limited number of available returned samples no selection criteria were used to select the Apollo or Luna samples. This could potentially introduce bias into the analysis as in steps 2 and 3 the M³ data used was not selected randomly compared to the returned samples which are assumed to have been chosen at random. However, steps 2 and 3 are required to insure the region of interest has not been contaminated by ejector blankets from other impacts, therefore this potential bias is unavoidable in these techniques.

There is further bias in the returned Apollo samples as they generally contain low TiO₂ (this is discussed further in section 2.4—only 4 samples contain >8% TiO₂). Unfortunately, due to the limited number of the returned samples it is not possible to remove this bias.

After selecting the M³ data and the Apollo/Luna returned samples, the reflectance in the 750 nm channel and the ratio of the reflectance in the 540 nm/750 nm channel was plotted (Fig. 7). It is clear from the scatter plot in Fig. 7 that the selected data at different landing sites converge in an optimized origin in a similar way to the previously discussed FeO/TiO₂ abundance analysis by Lucey et al. (1995, 1998) using the Clementine data (Fig. 2). Based on Fig. 7, the coordinate of the optimized origin is calculated: X₀ = 0.163, Y₀ = 0.57.

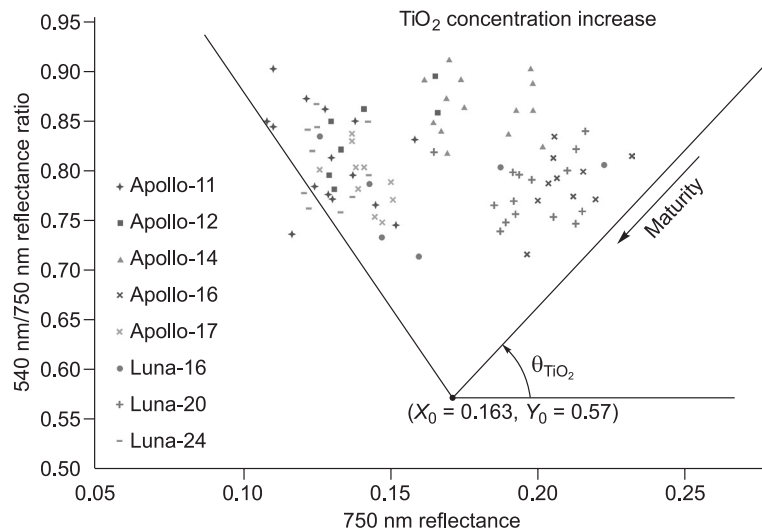


Fig. 7. Scatter plot of the spectral reflectance ratio (540 nm/750 nm) vs reflectance (750 nm) from microcraters around Apollo sampling points.

When the reflectance at 750 nm is greater than 0.163, the TiO₂ angle calculation formula is written as follows:

$$\theta_{\text{TiO}_2} = \arctan \left(\frac{\frac{R_{540\text{nm}}}{R_{750\text{nm}}} - 0.57}{R_{750\text{nm}} - 0.163} \right) \quad (5)$$

When the reflectance at 750 nm is less than 0.163, the TiO₂ angle calculation formula is written as follows:

$$\theta_{\text{TiO}_2} = \pi - \arctan \left(\frac{\frac{R_{540\text{nm}}}{R_{750\text{nm}}} - 0.57}{0.163 - R_{750\text{nm}}} \right) \quad (6)$$

When the reflectance at 750 nm = 0.163, the TiO₂ angle is $\theta_{\text{TiO}_2} = 1.57$.

Following the method of Lucey et al. (1995, 1998, 2000), a statistical relationship was built between the TiO₂ angle and the TiO₂ content of the Apollo/Luna returned samples measured in the laboratory by chemical analysis. The statistical relationship was derived using a least squares fitting algorithm (Fig. 8) and found to be:

$$\text{TiO}_2 \% = 0.1089 \times \theta_{\text{TiO}_2}^{6.6535} \quad (7)$$

Compared with the actual value of the points used to generate the fit, the derived relationship has a high correlation coefficient of 0.92. Using Eq. 7, analysis of the TiO₂ content from M³ data was made and it shows a comparison of the retrieved TiO₂ content using the two different methods discussed in this chapter, e.g., the adapted Lucey et al. (1995, 1998) method and the Shkuratov et al. (1999) method.

It can be seen that the Shkuratov et al. (1999) method produces much lower TiO₂ abundances than the Lucey et al. (1995, 1998) method. This is a systematic deviation that can also be observed from Shkuratov et al. (1999) and the Lucey et al. (1995, 1998) papers as the former method presented much lower Ti abundance (0–9%) than the latter (0–18%). As the returned Apollo and Luna samples generally have very low TiO₂ abundances (only 4 returned samples have TiO₂ > 8%, most samples contain 1–3% TiO₂), the Shkuratov et al. (1999) method is preferred. Also given that the Lucey et al. (1995, 1998) method operates only with two reflectance's, the Shkuratov et al. (1999) method is preferred as it uses more reflectance data including telescopic data.

Using a comparison with returned lunar soil samples from Apollo, Luna and Surveyor Landing Sites to estimate error

Comparison of the M³ derived FeO and TiO₂ abundances with values measured from the returned samples of various landing sites is possible (Shkuratov et al., 1999). Table 2 compares the FeO and TiO₂ abundances of returned Apollo/Luna samples with the derived M³ TiO₂ and FeO abundances calculated in this chapter and with the previously derived values from the Clementine data. Except for the TiO₂ abundance from two extremely high abundance samples (Surveyor 5 and Apollo 11–7.6% and 7.4%), the M³ data matches the returned sample data at all other landing sites with a deviation of less than ±2.8%, based on which we can estimate the error in this approach. The discrepancy in the high TiO₂ regions is likely due to, too few high TiO₂ samples (only four samples) which limits the accuracy of the extrapolation. It is hard to compare the new approach developed in this chapter to the Lucey et al. (1995, 1998, 2000) Clementine derived abundances since they do not quote an uncertainty, however, the results are provided in Table 2 for the reader's interest.

Table 2 compares the abundances of FeO and TiO₂ in the returned samples to the values derived from M³. However, the returned samples used in this table were also used in the technique to the derived abundance levels from the M³ data. It would therefore be more appropriate to compare the derived M³ abundances to returned samples that were not used in the derivation process, which are marked as italic in Table 2 (five samples).

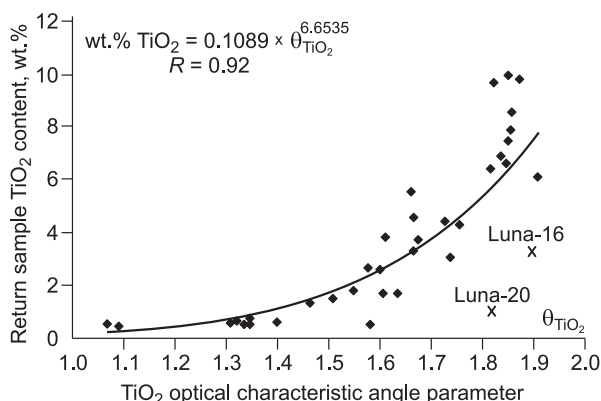


Fig. 8. Fitting of TiO₂ content against the TiO₂ characteristic angle parameter. Errors of the plotted data are evenly distributed and will not affect the fitting.

Table 2. Comparison with samples returned from the Apollo, Luna and Surveyor landing sites as well as the Clementine retrieved values. Values given in bold have been calculated by the author as a part of this work, all other values have been taken from Shkuratov et al. (1999). Values given in italic are the comparison with unused soil data from the Apollo and Surveyor Landing Sites

Landing site	Sample TiO ₂ (%)	M ³ TiO ₂ (%)	*Clementine TiO ₂ (%)	Sample FeO (%)	M ³ FeO (%)	*Clementine FeO (%)	References
Apollo-11	7.40	2.23	11.7±0.7	15.8	14.8	13	(Florensky et al., 1981; Lunar Sourcebook, 1991; King, 1976; Nawa et al., 1979)
Apollo-12	2.68	2.65	6.4±0.5	15.7	16.0	13.5	
Apollo-14	1.72	1.70	1.8±0.3	10.4	12.8	8.6	
Apollo-15 (maria)	<i>1.64</i>	2.32	<i>1.7±0.6</i>	<i>15.2</i>	15.1	<i>12.9</i>	
Apollo-16	0.55	0.88	0.8±0.1	5.0	7.8	4.0	(LSPET, 1973)
Apollo-17 (highland)	<i>0.90</i>	0.95	<i>3.7±1.8</i>	<i>8.1</i>	8.6	<i>6.9</i>	
Luna-16	3.36	2.71	6.4±0.6	16.7	14.8	13.0	(Florensky et al., 1981; Lunar Sourcebook, 1991)
Luna-20	0.47	0.74	1.3±0.1	7.4	6.9	5.8	
Luna-24	1.15	2.52	5.0±0.5	20.6	17.8	15.1	(Florensky et al., 1981; Lunar Sourcebook, 1991)
Surveyor-5	<i>7.60</i>	2.01	<i>N/A</i>	<i>12.1</i>	13.8	<i>N/A</i>	(Mason and Melson, 1970)
Surveyor-6	<i>3.50</i>	2.41	<i>N/A</i>	<i>12.4</i>	13.2	<i>N/A</i>	
Surveyor-7	<i>0.50</i>	0.75	<i>N/A</i>	<i>5.5</i>	6.9	<i>N/A</i>	

*Clementine TiO₂ content values and errors were obtained from Korokhin et al. (2008), and Clementine FeO content values were obtained from Pinet et al. (1997). None of the authors provided content retrieval errors of Clementine FeO in their papers (Hapke, 1981; Lucey et al., 1995, 1996, 1998, 2000; Blewett et al., 1997; Shkuratov et al., 1999). The error range of Clementine and M³ should be of the same magnitude.

It is noticed that the Clementine derived FeO content was systematically 1–2% lower in all the returned samples than the laboratory measurements. The M³ derived content compared better with the returned Apollo samples and was within ±2.8% of the laboratory measurements, without systematic biases. The Clementine derived TiO₂ abundance was systematically 0.1–4% higher than the laboratory measurements of the returned samples. The M³ derived TiO₂ compared well (±0.6%) with the laboratory measurements of the returned samples except for samples with high TiO₂ content. Again, this discrepancy in the high TiO₂ regions can be improved if samples with higher TiO₂ can be provided in the future.

LUNAR REGOLITH DENSITY INFORMATION

The sensitivity analysis showed that the bulk density of the lunar soil is another major cause of uncertainty for MRM modeling. There has been considerable effort expended over the years to estimate the spatial distribution of the bulk density of the lunar soil (Carrier et al., 1991; Pinet et al., 1997). However, lunar soil bulk density is yet to be globally measured by instrumentation (the depth of GRAIL data at 40 km is too deep for this research; this research studied only the top 2 m) (Zuber et al., 2013). Using this for the global lunar surface may introduce error into the microwave data inversion (Chapter 6), as the Moon's density varies between the highland and the maria (Carrier et al., 1991; Pinet et al., 1997).

The Apollo missions provided the only direct measurements of the lunar soil bulk density; however, they only provide data at discrete points and do not provide global coverage. Core tube samples of the upper lunar regolith were returned from all Apollo sites; however, the landing sites of the Apollo missions were limited to the near side of the lunar surface and equatorial regions. Only one mission (Apollo 16) landed in a typical highland region. Therefore, the lunar soil bulk density measurements made by the Apollo missions may not fairly represent the global bulk density of the lunar surface (Carrier et al., 1991).

As the Moon's density varies between the highland and the maria (Carrier et al., 1991; Pinet et al., 2012), the bedrock density is allowed to vary between the maria and highlands and is assumed to be proportional to the upper crust density at the same location. The latter can be estimated using the empirical correlation of Huang and Wieczorek (2012):

$$\rho = 0.0273\text{FeO} + 0.011\text{TiO}_2 + 2.773 . \quad (8)$$

This relation is based on the estimated mineralogical norms and densities of the lunar samples and has a quoted uncertainty of less than 0.05 g/cm³ (Fa and Wieczorek, 2012). Because the maria regions usually have higher FeO and TiO₂ abundances than highland regions, Eq. 8 indicates higher density values for maria regions, which qualitatively agrees with previous research (Carrier et al., 1991; Pinet et al., 1997).

CONCLUSIONS

In this paper, VIS to NIR reflectance data acquired by the M³ instrument was used to investigate the mineralogy of the lunar surface. The FeO content based on M³ data was analyzed with the use of Lucey's model and compared to previous estimates. The derived FeO content also compared well with the measured FeO content of returned Apollo samples (deviation <±2.8%). The TiO₂ content based in the M³ was also analyzed using Lucey's approach and compared to previous estimates derived from the Clementine data. Although the M³ derived TiO₂ content compared well with the Clementine data, neither compared well with the measured TiO₂ content of returned Apollo samples (Lucey's method calculates TiO₂ content an order of magnitude higher than the Apollo samples). A second approach, the Shkuratov method, was used to derive the TiO₂ content from the M³ data and this method compared well with the returned Apollo sample measurements (deviation <±2.8%, except for high TiO₂ regions—greater than 7%). Thus, the Shkuratov derived TiO₂ will be used in the inverse scheme. The Shkuratov method is an empirical fit and more data and laboratory experiments are required to further constrain the empirical fit.

I improved Lucey's method and applied it on M³ instrument because it increases the accuracy of previous global elemental abundance maps derived from Clementine (which had large uncertainties) and provides an important test of different reduction approaches. The first superiority of this method is that Clementine derived FeO content systematically lower (1–2%) in all the returned samples than the laboratory measurements, while M³ derived content compared better. The second of which is that Clementine derived TiO₂ abundance systematically higher (0.1–4%) than the laboratory measurements of the returned samples, while M³ derived TiO₂ compared well. This method can be used in other planetary exploration and eventually become a systematic method in the future.

Acknowledgments. First of all, my deepest thanks go to my supervisor, Professor Neil Bowles from the University of Oxford, for his explicit advice on the sharpening of my ideas, and his tolerance and patience in reading and correcting my drafts. Besides, I am grateful to Mr. Chi Shen from Shaoxing University, who gave me plenty of valuable suggestions in improving the accuracy of this paper. Also, I'm obliged to my family and colleges who accompanied me these years, giving me the support that I will never forget.

Finally, my sincere gratitude goes to those who have devoted time reading this thesis and given me many suggestions, which will benefit my study and work in the future.

REFERENCES

- Bhatt, M., Mall, U., Bugiolacchi, R.,** 2011. Iron mapping method based on 2 μm absorption parameters using SIR-2 data on-board Chandrayaan-1, in: EPSC-DPS Joint Meeting (2–7 October 2011, Nantes), Vol. 6, p. 441.
- Blewett, D.T., Lucey, P.G., Hawke, B.R., Bradley L.J.,** 1997. Clementine images of the lunar sample-return stations: Refinement of FeO and TiO₂ mapping techniques. *J. Geoph. Res. Planets* 102 (E7), 16,319–16,325.
- Boardman, J.W., Pieters, C.M., Green, R.O., Lundeen, S.R., Varanasi, P., Nettles, J., Petro, N., Isaacson, P., Besse, S., Taylor, L.A.,** 2011. Measuring moonlight: An overview of the spatial properties, lunar coverage, selenolocation, and related Level 1B products of the Moon Mineralogy Mapper. *J. Geoph. Res. Planets* 116 (E6), E00G14.
- Carrier, W.D., Olhoeft, G.R., Mendell, W.,** 1991. Physical properties of the lunar surface, in: Heiken, G., Vaniman, D., French, B.M. (Eds.), *Lunar Sourcebook*. Cambridge University Press, Cambridge, pp. 475–594.
- Clark, R., Pieters, C.M., Green, R.O., Boardman, J., Buratti, B.J., Head, J.W.III, Isaacson, P.J., Livo, K.E., McCord, T.B., Nettles, J.W., Petro, N.E., Sunshine, J.M., Taylor, L.A.,** 2010. Water and hydroxyl on the Moon as seen by the Moon Mineralogy Mapper (M³), in: 41st Lunar Planet Sci. Conf., Abstracts, No. 2302.
- Cloutis, E.A., McCormack, K.A., Bell, J.F., Hendrix, A.R., Bailey, D.T., Craig, M.A., Mertzman, S.A., Robinson, M.S., Riner, M.A.,** 2008. Ultraviolet spectral reflectance properties of common planetary minerals. *Icarus* 197 (1), 321–347.
- Dhingra, D., Pieters, C.M., Isaacson, P., Staid, M., Mustard, J., Klima, R., Taylor, L.A., Kramer, G., Nettles, J., M³ Team,** 2010. Spectroscopic signature of the high titanium basalts at Mare Tranquillitatis from Moon Mineralogy Mapper (M³), in: 41st Lunar Planet Sci. Conf., Abstracts, No. 2494.

- Fa, W., Wieczorek, M.A.**, 2012. Regolith thickness over the lunar nearside: Results from Earth-based 70-cm Arecibo radar observations. *Icarus* 218 (2), 771–787.
- Florensky, K.P., Barsukov, V.L.**, 1981. *Essays of Comparative Planetology* [in Russian]. Nauka, Moscow.
- Gillis, J.J., Jolliff, B.L., Korotev, R.L.**, 2004. Lunar surface geochemistry: Global concentrations of Th, K, and FeO as derived from lunar prospector and Clementine data. *Geochim. Cosmochim. Acta* 68 (18), 3791–3805.
- Green, R.O., Pieters, C., Mouroulis, P., Eastwood, M., Boardman, J., Glavich, T., Isaacson, P., Annadurai, M., Besse, S., Barr, D., Buratti, B., Cate, D., Chatterjee, A., Clark, R., Cheek, L., Combe, J., Dhingra, D., Essandoh, V., Geier, S., Goswami, J.N., Green, R., Haemmerle, V., Head, J., Hovland, L., Hyman, S., Klima, R., Koch, T., Kramer, G., Kumar, A.S.K., Lee, K., Lundeen, S., Malaret, E., McCord, T., McLaughlin, S., Mustard, J., Nettles, J., Petro, N., Plourde, K., Racho, C., Rodriguez, J., Ruyon, C., Sellar, G., Smith, C., Sobel, H., Staid, M., Sunshine, J., Taylor, L., Thaisen, K., Tompkins, S., Tseng, H., Vane, G., Varanasi, P., White, M., Wilson, D.**, 2011. The Moon Mineralogy Mapper (M³) imaging spectrometer for lunar science: Instrument description, calibration, on-orbit measurements, science data calibration and on-orbit validation. *J. Geophys. Res. Atmosph.* 116 (10), 1241–1249.
- Hapke, B.**, 1981. Bidirectional reflectance spectroscopy: I. Theory. *J. Geophys. Res. Solid Earth* 86 (B4), 3039–3054.
- Hartmann, W.K., Phillips, R.J., Taylor, G.J.**, 1986. *Origin of the Moon*. Edward Bros., Lunar Planetary Institute.
- Heiken, G.H., Vaniman, D.T., Bevan M.** (Eds.), 1991. *Lunar Sourcebook*. Cambridge University Press, Cambridge.
- Huang, Q., Wieczorek, M.A.**, 2012. Density and porosity of the lunar crust from gravity and topography. *J. Geophys. Res. Planets* 117 (E5), E05003.
- Kim, J., Wöhler, C., Hasebe, N., van Gasselt, S., Berezhnoy, A.A., Rodriguez, J.A.P., Grumpe, A.**, 2016. Lunar silicon distribution as observed by the Kaguya gamma-ray spectrometer and Chandrayaan-1 Moon Mineralogy Mapper (M³) calibration, in: 47th Lunar and Planetary Sci. Conf., Abstracts, No. 1473.
- King, E.**, 1976. *Space Geology (an Introduction)*. Wiley, New York.
- Korokhin, V.V., Kaydash, V.G., Shkuratov, Y.G., Stankevich, D.G., Urs, M.**, 2008. Prognosis of TiO₂ abundance in lunar soil using a non-linear analysis of Clementine and LSCC data. *Planet. Space Sci.* 56 (8), 1063–1078.
- Kramer, G.Y., Besse, S., Nettles, J.J., Combe, P., Clark, R.N., Pieters, C.M., Staid, M., Malaret, E., Boardman, J., Green, R.O., Head, J.W., McCord, T.B.**, 2011. Newer views of the Moon: Comparing spectra from Clementine and the Moon Mineralogy Mapper. *J. Geophys. Res. Planets* 116 (E6), E00G04.
- Lawrence, D.J., Feldman, W.C., Elphic, R.C., Little, R.C., Prettyman, T.H., Maurice, S., Lucey, P.G., Binder, A.B.**, 2002a. Iron abundances on the lunar surface as measured by the Lunar Prospector gamma-ray and neutron spectrometers. *J. Geophys. Res. Planets* 107 (E12), 13-1–13-26.
- Lawrence, D.J., Elphic, R.C., Feldman, W.C., Gasnault, O., Genetay, I., Maurice, S., Prettyman, T.H.**, 2002b. Small-area thorium enhancements on the lunar surface, in: 33rd Lunar and Planetary Sci. Conf., Abstract, No. 1970.
- Lawrence, D.J., Puetter, R.C., Elphic, R.C., Feldman, W.C., Hagerty, J.J., Prettyman, T.H., Spudis, P.D.**, 2007. Global spatial deconvolution of Lunar Prospector Th abundances. *Geophys. Res. Lett.* 34 (3), L03201.
- LSPET (Lunar Sample Preliminary Examination Team)**, 1973. Apollo 17 lunar samples: Chemical and petrographic description. *Science* 183, 659–672.
- Lucey, P.G., Taylor, G.J., Malaret, E.**, 1995. Abundance and distribution of iron on the Moon. *Science* 268 (5214), 1150–1153.
- Lucey, P.G., Blewett, D.T., Johnson, J.R., Taylor, G.J., Hawke, B.R.**, 1996. Lunar titanium content from UV-VIS measurements. *Lunar Planet Sci.* 27, 781–782.
- Lucey, P.G., Blewett, D.T., Hawke, B.R.**, 1998. Mapping the FeO and TiO₂ content of the lunar surface multispectral imagery. *J. Geophys. Res. Planets* 103 (E2), 3679–3699.
- Lucey, P.G., Blewett, D.T., Jolliff, B.L.**, 2000. Lunar iron and titanium abundance algorithms based on final processing of Clementine ultraviolet-visible images. *J. Geophys. Res. Planets* 105 (E8), 20,297–20,305.
- Lucey, P., Korotev, R.L., Gillis, J.J., Taylor, L.A., Lawrence, D., Campbell, B.A., Elphic, R., Feldman, B., Hood, L.L., Hunten, D., Mendillo, M., Noble, S., Papike, J.J., Reedy, R.C., Lawson, S., Prettyman, T., Gasnault, O., Maurice, S.**, 2006. Understanding the lunar surface and space-Moon interactions. *Rev. Mineral. Geochem.* 60 (1), 83–219.

Nawa, D.F., Philpotts, J.A., 1979. A lunar differentiation model in light of new chemical data on Luna 20 and Apollo 16 soils, in: Barsukov, V.L. (Ed.), *Regolith from the Highland Region of the Moon* [in Russian]. Nauka, Moscow, pp. 336–344.

Mason, B., Melson, W., 1997. *The Lunar Rocks*. Wiley, New York.

Nozette, S., Rustan, P., Pleasance, L.P., Kordas, J.F., Lewis, I.T., Park, H.S., Priest, R.E., Horan, D.M., Regeon, P., Lichtenberg, C.L., Shoemaker, E.M., Eliason, E.M., McEwen, A.S., Robinson, M.S., Spudis, P.D., Acton, C.H., Buratti, B.J., Duxbury, T.C., Baker, D.N., Jakosky, B.M., Blamont, J.E., Corson, M.P., Resnick, J.H., Rollins, C.J., Davies, M.E., Lucey, P.G., Malaret, E., Massie, M.A., Pieters, C.M., Reisse, R.A., Simpson, R.A., Smith, D.E., Sorenson, T.C., Vorder Breugge, R.W., Zuber, M.T., 1994. The Clementine mission to the Moon: Scientific overview. *Science* 266 (5192), 1835–1839.

Pieters, C.M., Head III, J.W., Isaacson, P., Petro, N., Runyon, C., Ohtake, M., Föing, B., Grande, M., 2008. Lunar international science coordination/calibration targets (L-ISCT). *Adv. Space Res.* 42 (2), 248–258.

Pieters, C.M., Goswami, J.N., Clark, R.N., Annadurai, M., Boardman, J., Buratti, B., Combe, J.P., Dyar, M.D., Green, R., Head, J.W., Hibbitts, C., Hicks, M., Isaacson, P., Klima, R., Kramer, G., Kumar, S., Livo, E., Lundeen, S., Malaret, E., McCord, T., Mustard, J., Nettles, J., Petro, N., Runyon, C., Staid, M., Sunshine, J., Taylor, L.A., Tompkins, S., Varanasi, P., 2009. Character and spatial distribution of OH/H₂O on the surface of the Moon seen by M³ on Chandrayaan-1. *Science* 326 (5952), 568–572.

Pinet, P.C., Shevchenko, V.V., Chevrel, S., 1997. Reiner gamma formation from Clementine uv-visible spectro-imaging data: the lunar chronology and iron content, in: 28th Lunar and Planetary Sci. Conf., Abstracts, pp. 14–31.

Shkuratov, Y.G., Kaydash, V.G., Opanasenko, N.V., 1999. Iron and titanium abundance and maturity degree distribution on lunar nearside. *Icarus* 137 (2), 222–234.

Vaughan, D.J., Burns, R.G., 1973. Low oxidation states of FeO and TiO₂ in the Apollo 17 orange soil. *EOS Trans. AGU* 54, 618–620.

Zuber, M.T., Smith, D.E., Lehman, D.H., Hoffman, T.L., Asmar, S.W., Watkins, M.M., 2013. Gravity recovery and interior laboratory (GRAIL): Mapping the Lunar interior from crust to core, in: Zuber, M.T., Russel, C.T. (Eds.), *GRAIL: Mapping the Moon's Interior*. Springer, pp. 3–24.

*Рекомендована к печати 23 октября 2018 г.
Н.Л. Добрецовым*

*Поступила в редакцию
22 мая 2019 г.*